

Paleodepositional environment and salt lake organic matter enrichment model of the Paleogene Linhe Formation in the Linhe Sag of the Hetao Basin

Liu Wei

QingHai Salt Lake Industry Co.,Ltd. China

Abstract: The well-developed mudstone and gypsum mudstone in Oligocene Linhe Formation (E3l) in the Hetao Basin are the main source rocks. However, the sedimentary environment and organic matter (OM) enrichment factors of E3l are not clear, which inhibit the prediction of hydrocarbon source rock distribution and resource calculation. The major and trace elements, X-ray diffraction (XRD), scanning electron microscopy, total organic carbon (TOC), Rock-Eval pyrolysis, saturated hydrocarbon gas chromatography-mass spectrometry (GC-MS) experiments were analyzed.

Keywords: Saline lake, organic enrichment, palaeoenvironment, source rock, Hetao Basin

1. Introduction

At present, the typical paleo-sedimentary environment and development model of lacustrine source rocks include large-scale deep-water anoxic lake basin model, high-salinity closed lake basin model, medium-deep tropical lake basin model and oligotrophic lake basin model. According to the sedimentary theory and previous research experience. The study of paleo-sedimentary environment mainly includes terrestrial input, redox conditions, paleo-salinity, paleoclimate, paleoproductivity, sedimentation rate and paleowater depth etc. Terrestrial inputs introduce plant detritus but also dilute the availability of OM. The reduction environment reduces the consumption and is conducive to the enrichment of OM. Adequate salinity is more conducive to biogenesis. Climate affects water evaporation and is closely related to the preservation. Paleoproductivity directly affects the hydrocarbon generation capacity. Sedimentation rate and paleo-water depth affect the redox and productivity of water, and further affect the development of OM.

At present, few studies on source rocks of Linhe Formation (E_{3l}) in Linhe Depression of Hetao Basin. The seismic facies study of source rock distribution, organic geochemistry, oil source correlation, and structural prediction of exploration prospects etc. The ancient sedimentary environment characteristics of mudstone and gypsum mudstone in E_{3l} have not been studied systematically. There is no distinction between their sedimentary environments. This is not conducive to correctly assessing the hydrocarbon generation capacity and distribution characteristics. In addition, the ancient sedimentary environment and development model of

saline lake source rocks in E_{3l} are clarified. It can not only enrich the theoretical research of saline lake source rocks, but also enrich the content of sedimentology, environmental chemistry and petroleum geology.

2. Geological background

The Hetao Basin has an area of about 40,000 square kilometers, between the Yinshan Mountains and the Helan Mountains, and adjacent to the Ordos Basin (Fig.1a). In the regional tectonic position, the basin is sandwiched between the North China plate, the Alxa plate and the Central Asian orogenic belt. Linhe depression is located in the western part of the basin, has the largest area of 2.43 * 10⁴ km², which is the main sedimentary depression and oil-bearing area (Fig.1a, b). It can be divided into Jilantai sag in the south and Bayannaer sag in the north bounded. It has the structural characteristics of east-west zoning and north-south zoning. Among them, the east-west direction of Bayannaer sag can be divided into central broken belt and the Huanghe depression (Fig. 1b). Jilantai sag is divided into Jixi depression and Jibei uplift. The basement of the basin is the metamorphic rock series of the Paleoproterozoic-Archaean Wulashan Group. Its stratigraphic distribution is shown in Fig. 1c. Linhe Formation is a better source rock, while Wuyuan Formation is a better cap rock.

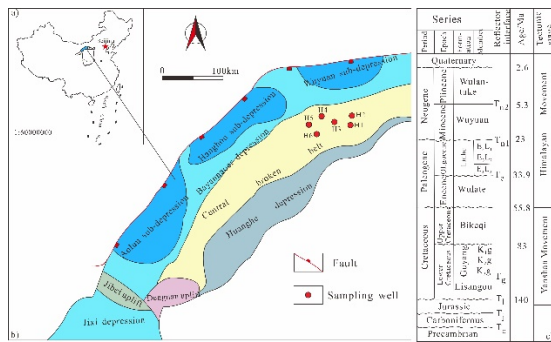


Fig. 1 Geographical location map (a), tectonic unit division map (b, modified from Zhang et al., 2020), and stratigraphic column map (c, modified from Li et al., 2022) of Hetao Basin

3. Sample and method

A total of 85 core samples were collected for experiments. Whole-rock mineral and clay component analysis via X-ray diffraction (XRD) was carried out for 7 samples. A total of 42 samples (23 mudstones and 19 gypsum mudstones) were used for total organic carbon (TOC), Rock-Eval pyrolysis and saturated hydrocarbon gas chromatography - mass spectrometry (GC-MS). We collected 36 core data (10 mudstones, 11 sandstones and 15 gypsum mudstones) from Linhe Formation of well H6 to carry out major and trace element analysis experiments. Scanning electron microscope analysis was carried out on two gypsum mudstone samples from well H6. The sampling location is shown in Fig.1b. The main trace element sampling diagram and core photos are shown in Fig.2. Because both Fig.2 (a) and Fig.2 (b) are sandstones, this section is not continuously sampled. The lithology of LH-13, LH-14 and LH-15 is gypsum-bearing argillaceous siltstone, which is summarized to gypsum mudstone in data processing.

3.1 XRD and Scanning electron microscope experiment

Instrument model: BRUKER D8 ADVANCE X-ray diffraction (XRD), sample 50mg, 200 mesh. According to the obtained spectra, quantitative analysis was performed using OriginLab Origin 2019 b software.

Application of traditional scanning electron microscope (referred to as scanning electron microscope, SEM) technology, model FEI NOVA NANO450, block sample length, width and height of less than 10mm, before scanning the sample end face using argon ion polishing.

3.2 TOC, Rock-Eval, GC-MS

Before analyzing, the samples were washed and dried with methanol / dichloromethane (1/9) solution and grinded into powder. Total organic carbon (TOC) analysis using LECO CS-125 carbon sulfur analyzer, specific analysis steps can refer to Xiao et al., 2021. After the air in the instrument was removed by helium, it was analyzed by Rock-Eval II instrument and heated to 600 °C. The pyrolysis parameters were recorded according to the analysis steps of Su et al., 2021.

GC / MS analysis was performed on Agilent 6890 chromatographic column with Agilent 5975 mass spectrometer detector. The saturated hydrocarbon was separated on a 30 m-long HP-5MS elastic silica capillary column (0.25 mm in diameter and 0.25 μm in wall thickness). Gas chromatography heating program: 50 °C constant temperature 1 min, 3 °C / min to 310 °C, constant temperature 30 min. He carrier gas, constant current mode, flow rate 1.0 mL / min.

3.3 Major and trace element analysis experiments

Analysis of trace boron by sodium hydroxide melt inductively coupled plasma mass spectrometry: The instrument used is inductively coupled plasma mass spectrometry (model 7900). The sample was weighed into the nickel crucible, and the sodium hydroxide flux was added to the sample. After fully mixing, it was melted at high temperature. After cooling, the melt was dissolved in deionized water and diluted to 100 mL. An equal amount of HCl was added to the solution, fully mixed, and analyzed by inductively coupled plasma mass spectrometry. After the spectral interference between elements is corrected, it is the final analysis result.

4. Results

4.1 Mineralogical characteristics

By analyzing the whole rock and clay mineral components of mudstone, gypsum mudstone and sandstone (Fig. 2), it can be found that the mineral component contents are quite different. The mudstone samples are dominated by clay minerals (averaging 51 %), followed by quartz (22.5 %), with a certain content of plagioclase (6.5 %) and calcite (26 %). Pyrite (6.3 %) was detected, with a small amount of potassium feldspar and analcite. There are more anhydrite and quartz in the gypsum mudstone samples, and the aragonite content of well H1 is 37 %. The content of quartz in sandstone is 50 %, and the content of silicate and carbonate minerals is similar (Fig.2a). The clay minerals are dominated the illite/ montmorillonite (I/S) layer. Compared with mudstone, the content of illite in gypsum mudstone is higher (Fig.2b). Pyrite and gypsum were detected by scanning electron microscopy and energy spectrum (Fig.3), plus high I/S in clay minerals. These characteristics indicate that the source rocks of E31 in Linhe Depression of Hetao Basin are in a reducing environment.

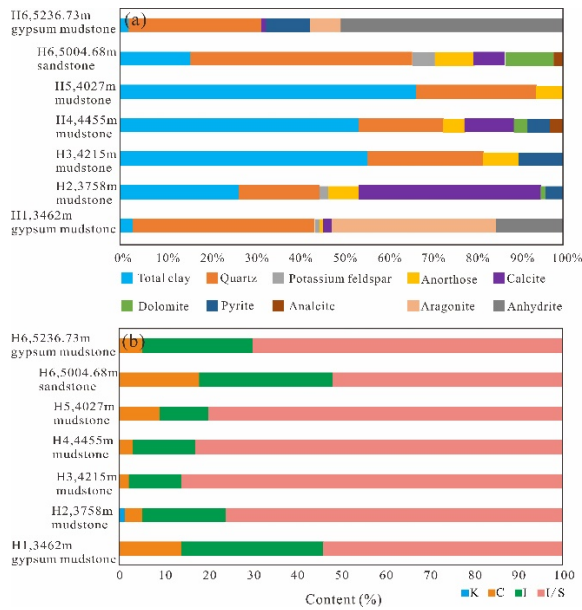


Fig. 2 Whole rock mineral content bar chart (a), clay mineral content bar chart (b)

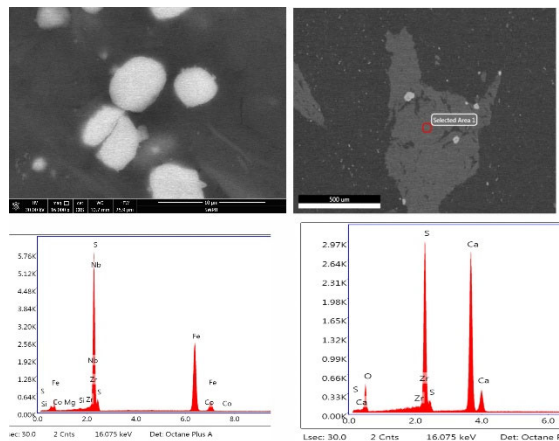


Fig. 3 Scanning electron microscope photos and energy spectrum of 5236.73 m sample from well H6

4.2 Organic geochemistry

Table 1 summarizes geochemical data of source rocks. The TOC represents the total amount of all organic matter in the rock. The S_1 represents free hydrocarbon (mg / g), liquid hydrocarbon content per unit mass of source rock detected at 300 ° C. The S_2 (mg / g) represents the amount of kerogen cracked by heating in source rocks from 300 to 600 ° C. The hydrogen index (HI) is $S_2 / TOC * 100\%$. The maximum temperature of pyrolysed hydrocarbon (Tmax) represents the temperature corresponding to the highest point of S_2 peak, which can be used to indicate the maturity of OM. The TOC values of mudstone samples in the study area are 0.11% -2.97%, with an average of 0.95%. The S_1 value is between 0.04 mg/g and 0.89 mg/g, averaging 0.31 mg / g. The content of S_2 is from 0.11 mg/g to 18.76 mg/g, averaging 3.76 mg/g. The Tmax values are between 416 ° C and 435 ° C, with an average of 423 ° C. The average HI value is 293 mg HC / g TOC. Parameters of gypsum mudstone are similar to mudstone.

4.3 Geochemistry of elements

Table 2 summarizes the major element contents of well H6. The average value of the ratio of the main elements of mudstone, sandstone and gypsum mudstone to the elements of Union Carbide Corporation (UCC) is shown in Fig. 4. The content of SiO_2 in the main elements is high, with an average of 50.11 %, followed by Al_2O_3 and CaO. The content of Al_2O_3 is 3.40 % - 18.29 %, with an average of 10.89 %, and the content of CaO is 1.25 % -27.00 %, averaging 8.39 %.

Compared with UCC elements, SiO_2 elements in sandstone are relatively enriched, and other major elements are relatively depleted. The variation trend of elements in mudstone and gypsum mudstone is similar. But, the P_2O_5 in mudstone is relatively enriched, that in gypsum mudstone is relatively depleted (Fig. 7).

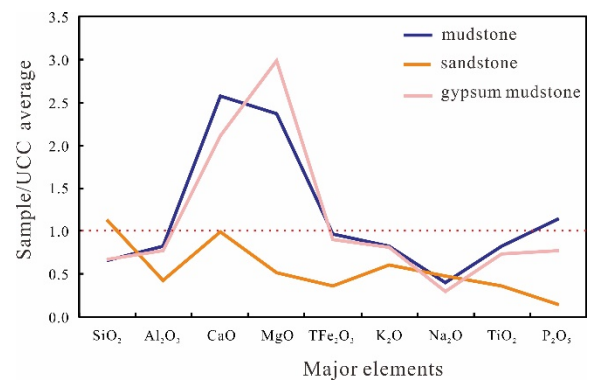


Fig. 4 The mean value line chart of major elements / UCC of different lithology in E3l of H6 well

5. Conclusions

There are two kinds of source rocks, mudstone and gypsum mudstone, in E3l of Hetao Basin, but their hydrocarbon generation potential is the same. By analyzing their sedimentary environment characteristics, the following conclusions can be drawn:

- (1) The correlation between Al_2O_3 and TiO_2 and TOC shows that terrestrial input is used as a diluent to reduce the content of OM, which is not conducive to enrichment. The effect of terrestrial input on mudstone dilution is greater than that of gypsum mudstone.
- (2) Pr/Ph , Pr/nC_{17} , Ph/nC_{18} , δU , $V / (V + Ni)$, Ce/La , U_{EF} and Mo_{EF} represent redox. The source rocks of E3l were in a reducing environment as a whole, and there were weak oxidation-reduction changes in the vertical direction. The more reducing the environment, the more conducive to enrichment of OM.
- (3) GI , Sr/Ba , $CaO / (CaO + Fe)$ and $MgO / Al_2O_3 * 100$ are used to qualitatively characterize the paleosalinity, and B is used for quantitative calculation. The analysis results show that E3l was in salt water environment, and there was water stratification on the profile. Paleosalinity promotes the enrichment of OM, which has a greater impact on gypsum mudstone.

In this study, good preservation conditions, including reduction conditions, water stratification, and hot and dry climate, were the main controlling factors for OM enrichment.

References

1. Adams, T. D., Haynes, J. R., Walker, C. T., 1965. Boron in holocene illites of the dovey estuary, wales, and its relationship to palaeosalinity in cyclothemsl. *Sedimentology* 4(3), 189.
2. Algeo, T.J., Lyons, T. W., 2006. Mo-total organic carbon covariation in modern anoxic marine environments: implication for analysis of paleoredox and paleophy drographic conditions. *Palaeoceanography* 21(1), 1016. [10.1029/2004PA001112](https://doi.org/10.1029/2004PA001112).
3. Amils, R., Ellis-Evans, C. Hinghofer-Szalkay, H., 2007. Life in Extreme Environments. *Nature*, 409(6823),1092.
4. Algeo, T. J., Ingall, E., 2007. Sedimentary Corg: P ratios, paleocean ventilation, and phanerozoic atmospheric pO₂. *Palaeogeogr. Palaeoclimatol. Palaeoecol.* 256 (3-4),130-155. [10.1016/j.palaeo.2007.02.029](https://doi.org/10.1016/j.palaeo.2007.02.029).
5. Algeo, T.J., Tribovillard, N., 2009. Environmental analysis of paleoceanographic systems based on molybdenum–uranium covariation. *Chemical Geology*, 268 (3–4), 211-225. [10.1016/j.chemgeo.2009.09.001](https://doi.org/10.1016/j.chemgeo.2009.09.001).
6. Adegoke, A. K., Abdullah, W. H., Hakimi, M. H., Sarki Yandoka, B. M., 2015. Geochemical characterisation and organic matter enrichment of Upper Cretaceous Gongila shales from Chad (Bornu) Basin, northeastern Nigeria: Bioproductivity versus anoxia conditions 135, 73-87. [10.1016/j.petro.2015.08.012](https://doi.org/10.1016/j.petro.2015.08.012)
7. Bom, M.H.H., Ceolin, D., Kochhann, K.G.D., Krahl, G., Fauth, G., Bergue, C.T., Savian, J.F., Strohschoen Junior, O., Simões, M.G., Assine, M.L., 2021. Paleoenvironmental evolution of the Aptian Romualdo Formation, Araripe Basin, Northeastern Brazil. *Global Planet. Change* 203, 103528. [10.1016/j.gloplacha.2021.103528](https://doi.org/10.1016/j.gloplacha.2021.103528)
8. Compton, J. S., 1988. Degree of supersaturation and precipitation of organogenic dolomite. *Geology* 16(4), 318-321. [10.1130/0091-7613\(1988\)016<0318:DOSAPO>2.3.CO;2](https://doi.org/10.1130/0091-7613(1988)016<0318:DOSAPO>2.3.CO;2).
9. Copetti, D., Guyennon, N., Buzzi, F., 2020. Generation and dispersion of chemical and biological gradients in a large-deep multi-basin lake (Lake Como, north Italy): The joint effect of external drivers and internal wave motions. *Science of The Total Environment* 749(20), 141587. <https://doi.org/10.1016/j.scitotenv.2020.141587>
10. Cheng, D. W., Zhou, C. M., Zhang, Z. J., Yuan, X. J., Liu, Y. H., Chen, X. Y., 2022.